Supplementary Material for:

Untangling Sources of Error in the Density-Functional Many-Body Expansion

Dustin R. Broderick and John M. Herbert,*
Department of Chemistry & Biochemistry,
The Ohio State University, Columbus, Ohio, 43210 USA

February 27, 2025

Contents

List of Tables

List of Figures

*herbert@chemistry.ohio-state.edu

1 Tables

Table S1: Errors in ion–water interaction energies ΔE_{int} for $F^-(H_2O)_{15}$, computed using DFT/aug-cc-pVDZ in various quadrature grids and referenced to a benchmark using EML(250,974).

Functional	Grid	Mean Error[a]	
		kcal/mol[b]	%
SCAN	SG-2	-0.01 ± 0.02	0.01
	SG-3	-0.10 ± 0.01	0.09
	EML(75, 302)	0.01 ± 0.01	-0.00
	EML(99, 590)	-0.06 ± 0.01	0.05
r^{2}SCAN	SG-2	-0.03 ± 0.02	0.03
	SG-3	-0.12 ± 0.01	0.11
	EML(75, 302)	-0.01 ± 0.00	0.01
	EML(99, 590)	-0.00 ± 0.00	0.00

[a]With respect to the EML(250,974) value for the same functional, averaged over 11 geometries. [b]Uncertainty represents one standard deviation.

Table S2: Errors in ion–water interaction energies ΔE_{int} for $Cl^-(H_2O)_{15}$, computed using DFT/aug-cc-pVDZ in various quadrature grids and referenced to a benchmark using EML(250,974).

Functional	Grid	Mean Error[a]	
		kcal/mol[b]	%
SCAN	SG-2	0.05 ± 0.09	-0.07
	SG-3	0.02 ± 0.03	-0.03
	EML(75, 302)	0.08 ± 0.02	-0.10
	EML(99, 590)	-0.03 ± 0.01	0.04
r^2SCAN	SG-2	0.02 ± 0.09	-0.03
	SG-3	0.00 ± 0.03	0.00
	EML(75, 302)	-0.01 ± 0.01	0.01
	EML(99, 590)	-0.00 ± 0.00	0.00

[a]With respect to the EML(250,974) value for the same functional, averaged over 11 geometries. [b]Uncertainty represents one standard deviation.

Table S3: Combinatorial coefficients for the subsystems arising for MBE(n) calculations with $n = 1$–5 and $N = 16$ monomers.[a]

k	n				
	1	2	3	4	5
1	1	−14	91	−364	1001
2		1	−13	78	−286
3			1	−12	66
4				1	−11
5					1

[a]According to eq. 4.

Table S4: MBE(n) errors ion–water interaction energies at the HF/aug-cc-pVTZ level, $n = 1$–5.

Cluster	n	Mean Error[a] (kcal/mol)
$F^-(H_2O)_{15}$	2	-20.7 ± 3.8
$F^-(H_2O)_{15}$	3	2.7 ± 0.8
$F^-(H_2O)_{15}$	4	-0.7 ± 0.3
$F^-(H_2O)_{15}$	5	1.4 ± 0.2
$Cl^-(H_2O)_{15}$	2	-9.9 ± 1.5
$Cl^-(H_2O)_{15}$	3	1.5 ± 0.5
$Cl^-(H_2O)_{15}$	4	-0.8 ± 0.2
$Cl^-(H_2O)_{15}$	5	1.7 ± 0.2

[a]Averages across cluster geometries. Uncertainties represent one standard deviation.

Table S5: MBE(n = 1–5) errors in ion–water interaction energies for $F^-(H_2O)_{15}$ using DFT/aug-cc-pVDZ calculations with various quadrature grids.

Functional	n	Mean Error (kcal/mol)[a]					
		SG-1	SG-2	SG-3	EML(50, 194)	EML(75, 302)	EML(99, 590)
PBE	2	−38.8 ± 4.1	−38.6 ± 4.2	−40.0 ± 4.2	−38.8 ± 4.2	−38.8 ± 4.2	−38.8 ± 4.2
PBE	3	39.2 ± 1.8	36.8 ± 2.5	42.8 ± 2.1	39.2 ± 2.1	39.4 ± 2.0	39.4 ± 2.0
PBE	4	−71.9 ± 5.3	−61.7 ± 9.0	−81.9 ± 5.6	−72.0 ± 5.6	−73.3 ± 5.4	−73.4 ± 5.3
PBE	5	115.5 ± 15.2	89.7 ± 25.6	139.3 ± 15.2	116.1 ± 15.5	120.6 ± 14.6	120.7 ± 14.2
SCAN	2	−31.8 ± 4.2	−31.9 ± 4.2	−32.5 ± 4.2	−31.8 ± 4.2	−32.1 ± 4.2	−32.1 ± 4.2
SCAN	3	14.7 ± 1.3	13.8 ± 2.0	16.5 ± 1.5	14.8 ± 1.5	15.2 ± 1.5	15.2 ± 1.5
SCAN	4	−15.4 ± 3.2	−11.1 ± 6.8	−20.6 ± 2.2	−15.7 ± 2.6	−17.4 ± 2.0	−17.4 ± 1.9
SCAN	5	8.2 ± 8.1	−2.4 ± 18.9	21.3 ± 4.0	9.1 ± 6.1	14.2 ± 3.9	14.2 ± 3.5
r^2SCAN	2	–	−31.5 ± 4.2	−32.1 ± 4.2	–	−31.6 ± 4.2	−31.6 ± 4.2
r^2SCAN	3	–	13.7 ± 2.0	16.3 ± 1.5	–	15.1 ± 1.5	15.1 ± 1.4
r^2SCAN	4	–	−11.0 ± 6.8	−20.4 ± 2.1	–	−17.2 ± 2.0	−17.2 ± 1.9
r^2SCAN	5	–	−2.5 ± 19.0	20.9 ± 3.9	–	13.8 ± 3.8	13.9 ± 3.5
ωB97M-V	2	–	−26.6 ± 4.0	−27.3 ± 4.0	–	−26.5 ± 4.0	−26.5 ± 4.0
ωB97M-V	3	–	7.5 ± 1.3	10.1 ± 1.2	–	8.1 ± 1.2	8.1 ± 1.2
ωB97M-V	4	–	−2.5 ± 3.5	−9.8 ± 1.1	–	−5.6 ± 0.9	−5.6 ± 0.8
ωB97M-V	5	–	−7.7 ± 10.1	8.4 ± 2.0	–	0.9 ± 1.2	1.0 ± 1.0
ωB97X-V	2	–	−25.7 ± 4.0	−25.7 ± 4.0	−25.7 ± 4.0	−25.8 ± 4.0	−25.8 ± 4.0
ωB97X-V	3	–	5.9 ± 1.4	6.2 ± 1.1	6.0 ± 1.2	6.2 ± 1.1	6.2 ± 1.1
ωB97X-V	4	–	−3.0 ± 3.9	−4.6 ± 0.9	−3.5 ± 1.1	−4.4 ± 0.8	−4.4 ± 0.7
ωB97X-V	5	–	−2.0 ± 11.1	2.9 ± 1.7	−1.0 ± 2.8	2.0 ± 1.0	2.1 ± 0.8

[a] Averages across cluster geometries. Uncertainties represent one standard deviation.

Table S6: MBE(n = 1–5) errors in ion–water interaction energies for $Cl^-(H_2O)_{15}$ using DFT/aug-cc-pVDZ calculations with various quadrature grids.

Functional	n	Mean Error (kcal/mol)[a]					
		SG-1	SG-2	SG-3	EML(50, 194)	EML(75, 302)	EML(99, 590)
PBE	2	−22.4 ± 2.8	−21.3 ± 2.7	−22.6 ± 2.9	−22.5 ± 2.9	−22.6 ± 2.9	−22.6 ± 2.9
PBE	3	10.4 ± 2.2	1.0 ± 3.5	11.5 ± 1.9	11.1 ± 2.2	11.6 ± 2.0	11.7 ± 2.0
PBE	4	−4.9 ± 5.2	32.0 ± 18.0	−8.4 ± 4.9	−7.3 ± 3.2	−9.3 ± 1.3	−9.6 ± 1.3
PBE	5	−3.7 ± 15.0	−93.6 ± 53.0	5.4 ± 15.7	1.9 ± 8.2	8.3 ± 1.8	9.2 ± 1.7
SCAN	2	–	−16.7 ± 2.2	−17.7 ± 2.5	–	−17.7 ± 2.5	−17.7 ± 2.5
SCAN	3	–	−3.1 ± 3.6	5.1 ± 1.5	–	5.2 ± 1.2	5.2 ± 1.1
SCAN	4	–	29.5 ± 18.8	−3.1 ± 5.9	–	−3.3 ± 0.7	−3.6 ± 0.6
SCAN	5	–	−80.6 ± 55.0	2.2 ± 17.9	–	2.9 ± 1.2	3.9 ± 0.8
r^2SCAN	2	–	−16.2 ± 2.1	−17.2 ± 2.4	–	−17.2 ± 2.4	−17.2 ± 2.4
r^2SCAN	3	–	−3.2 ± 3.6	5.0 ± 1.5	–	5.0 ± 1.1	5.0 ± 1.1
r^2SCAN	4	–	29.4 ± 18.7	−3.1 ± 6.0	–	−3.3 ± 0.7	−3.6 ± 0.6
r^2SCAN	5	–	−80.2 ± 54.9	2.2 ± 18.1	–	3.1 ± 1.2	4.0 ± 0.8
ωB97M-V	2	–	−13.9 ± 1.9	−14.5 ± 2.0	–	−14.5 ± 2.0	−14.5 ± 2.0
ωB97M-V	3	–	−0.9 ± 1.9	3.9 ± 1.2	–	4.1 ± 1.0	4.1 ± 1.0
ωB97M-V	4	–	16.4 ± 9.2	−2.0 ± 3.2	–	−2.9 ± 0.6	−3.0 ± 0.5
ωB97M-V	5	–	−43.7 ± 26.6	1.2 ± 9.4	–	3.6 ± 0.8	4.1 ± 0.7
ωB97X-V	2	–	−14.1 ± 2.0	−14.4 ± 2.1	–	−14.4 ± 2.1	−14.4 ± 2.1
ωB97X-V	3	–	0.3 ± 2.1	3.3 ± 1.2	–	3.3 ± 0.9	3.3 ± 0.9
ωB97X-V	4	–	10.4 ± 10.2	−2.5 ± 3.5	–	−2.5 ± 0.5	−2.6 ± 0.4
ωB97X-V	5	–	−30.6 ± 29.5	3.9 ± 10.1	–	3.9 ± 0.8	4.4 ± 0.7

[a] Averages across cluster geometries. Uncertainties represent one standard deviation.

2 Figures

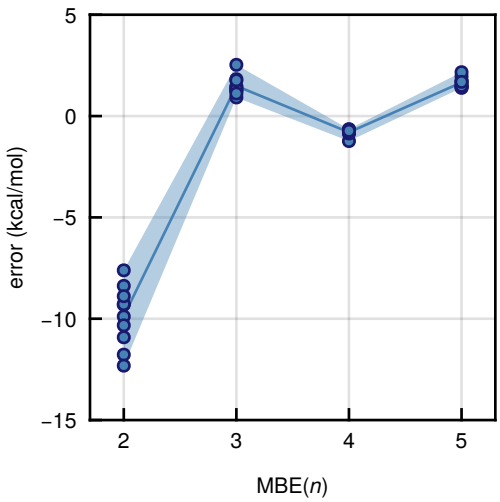

Figure S1: MBE(n) errors in ion–water interaction energies for 10 configurations of $Cl^-(H_2O)_{15}$ computed at the HF/aug-cc-pVDZ level. The solid line connects mean errors at each value of n and the shaded region highlights the range of the data.

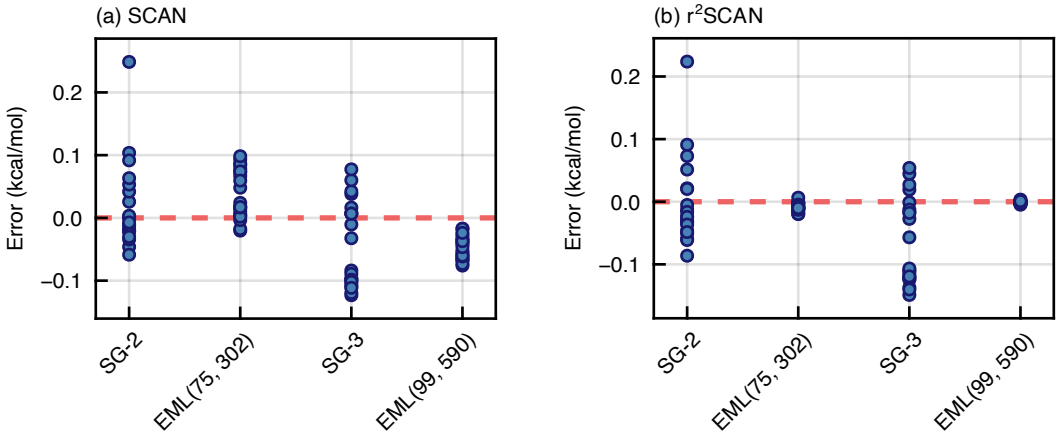

Figure S2: MBE(n) errors in ion–water interaction energies for 11 geometries of $F^-(H_2O)_{15}$ computed using (a) SCAN and (b) r^{2}SCAN with the aug-cc-pVDZ basis set and various quadrature grids. Errors are relative to a benchmark using EML(250,974).

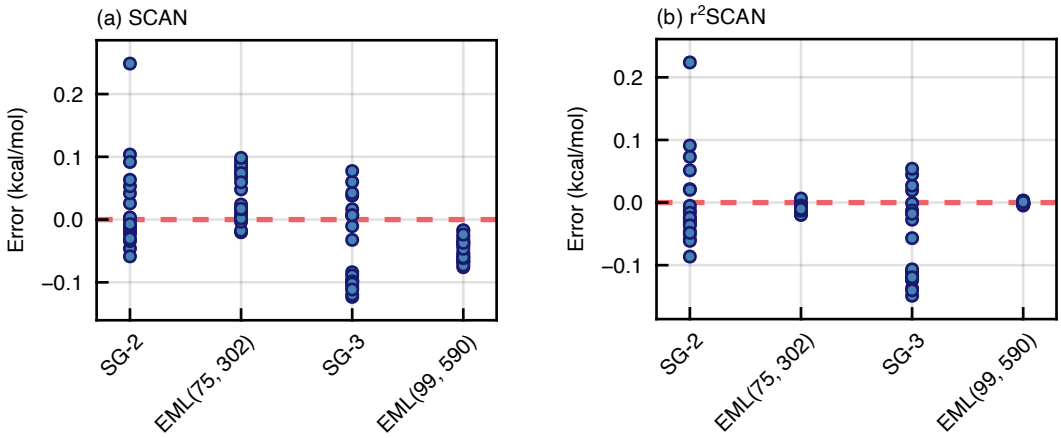

Figure S3: MBE(n) errors in ion–water interaction energies for 10 geometries of $Cl^-(H_2O)_{15}$ computed using (a) SCAN and (b) r^{2}SCAN with the aug-cc-pVDZ basis set and various quadrature grids. Errors are relative to a benchmark using EML(250,974).

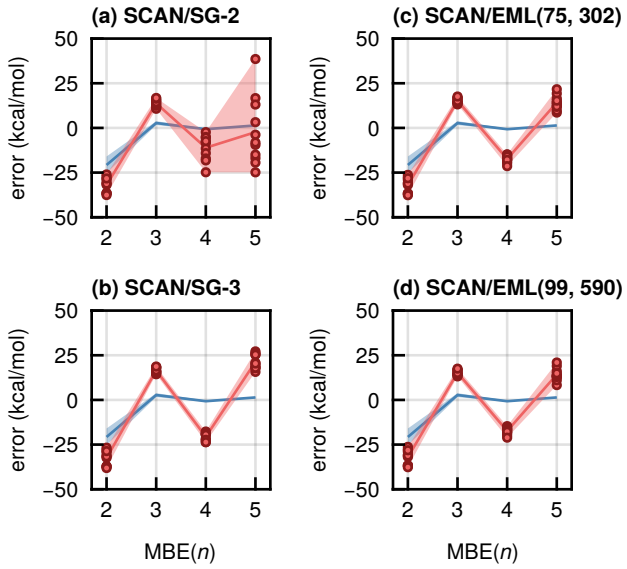

Figure S4: MBE(n) errors in ΔE_{int} (circles) for 11 configurations of $F^-(H_2O)_{15}$, computed at the SCAN/aug-cc-pVDZ level using various quadrature grids: (a) SG-1, (b) SG-2, (c) SG-3, (d) EML(50,194), (e) EML(75,302), (f) EML(99,590). The red shaded region and solid line connect the range of the errors and their mean, for each value of n. In blue are the HF/aug-cc-pVDZ errors from Fig. 1.

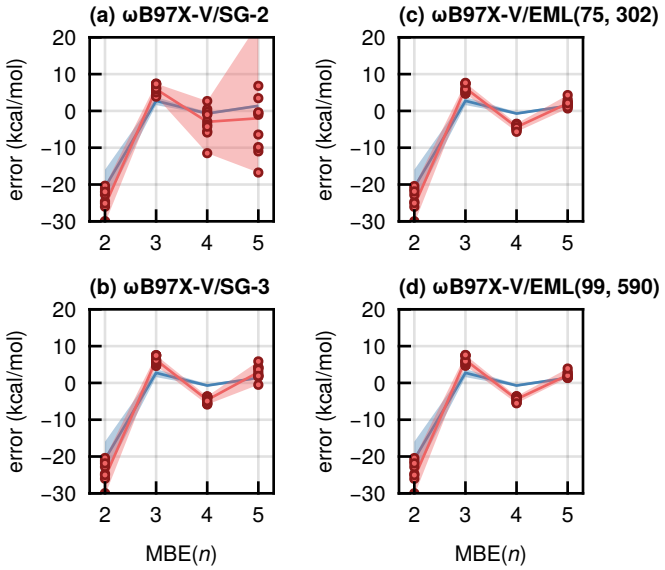

Figure S5: MBE(n) errors in ΔE_{int} (circles) for 11 configurations of $F^-(H_2O)_{15}$, computed at the ωB97X-V/aug-cc-pVDZ level using various quadrature grids: (a) SG-1, (b) SG-2, (c) SG-3, (d) EML(50,194), (e) EML(75,302), (f) EML(99,590). The red shaded region and solid line connect the range of the errors and their mean, for each value of n. In blue are the HF/aug-cc-pVDZ errors from Fig. 1.

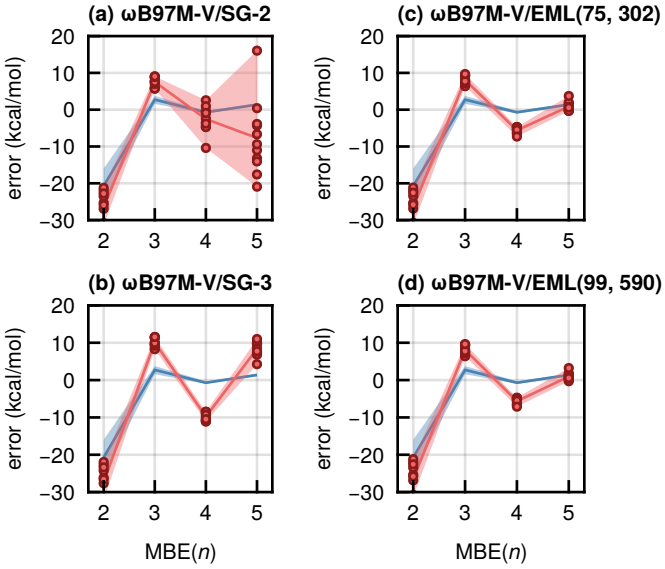

Figure S6: MBE(n) errors in ΔE_{int} (circles) for 11 configurations of $F^-(H_2O)_{15}$, computed at the ωB97M-V/aug-cc-pVDZ level using various quadrature grids: (a) SG-1, (b) SG-2, (c) SG-3, (d) EML(50,194), (e) EML(75,302), (f) EML(99,590). The red shaded region and solid line connect the range of the errors and their mean, for each value of n. In blue are the HF/aug-cc-pVDZ errors from Fig. 1.

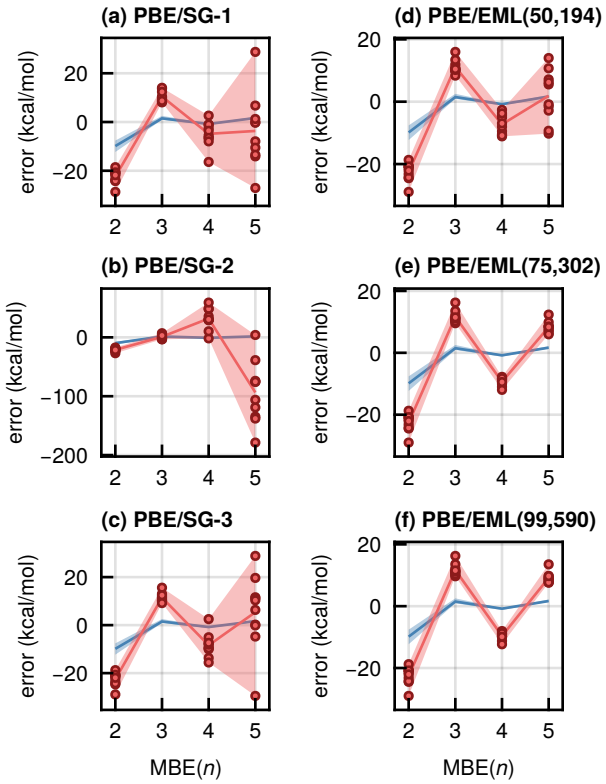

Figure S7: MBE(n) errors in ΔE_{int} (circles) for 10 $Cl^-(H_2O)_{15}$ cluster geometries, computed at the SCAN/aug-cc-pVDZ level using various quadrature grids: (a) SG-1, (b) SG-3, (c) SG-2, (d) SG-3, (e) EML(50,194), (e) EML(75,302), and (f) EML(99,590). The red shaded region and solid line connect the range of the errors and their mean, for each value of n. The blue line and shaded region represent the HF/aug-cc-pVDZ error distribution from Fig. S1.

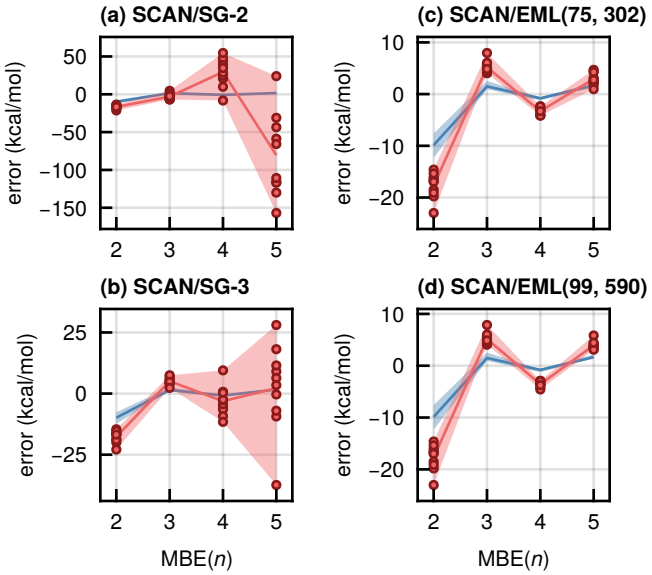

Figure S8: MBE(n) errors in ΔE_{int} (circles) for 10 $Cl^-(H_2O)_{15}$ cluster geometries, computed at the SCAN/aug-cc-pVDZ level using various quadrature grids: (a) SG-2, (b) SG-3, (c) EML(75,302), and (d) EML(99,590). The red shaded region and solid line connect the range of the errors and their mean, for each value of n. The blue line and shaded region represent the HF/aug-cc-pVDZ error distribution from Fig. S1.

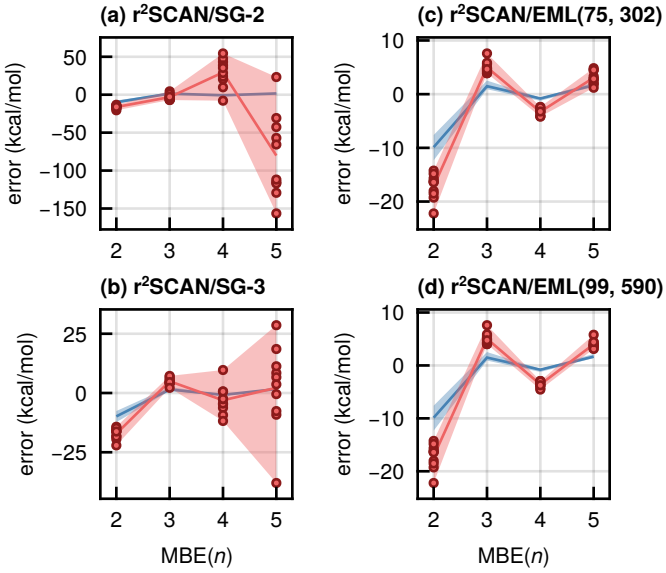

Figure S9: MBE(n) errors in ΔE_{int} (circles) for 10 $Cl^-(H_2O)_{15}$ cluster geometries, computed at the r^2SCAN/aug-cc-pVDZ level using various quadrature grids: (a) SG-2, (b) SG-3, (c) EML(75,302), and (d) EML(99,590). The red shaded region and solid line connect the range of the errors and their mean, for each value of n. The blue line and shaded region represent the HF/aug-cc-pVDZ error distribution from Fig. S1.

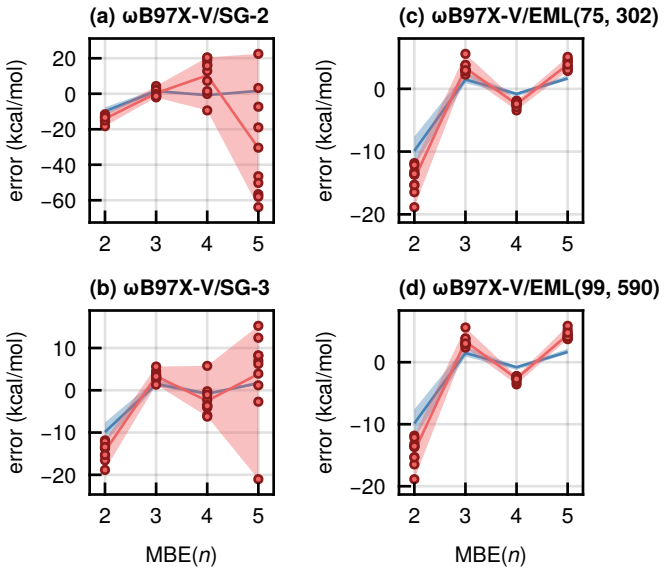

Figure S10: MBE(n) errors in ΔE_{int} (circles) for 10 $Cl^-(H_2O)_{15}$ cluster geometries, computed at the ωB97X-V/aug-cc-pVDZ level using various quadrature grids: (a) SG-2, (b) SG-3, (c) EML(75,302), and (d) EML(99,590). The red shaded region and solid line connect the range of the errors and their mean, for each value of n. The blue line and shaded region represent the HF/aug-cc-pVDZ error distribution from Fig. S1.

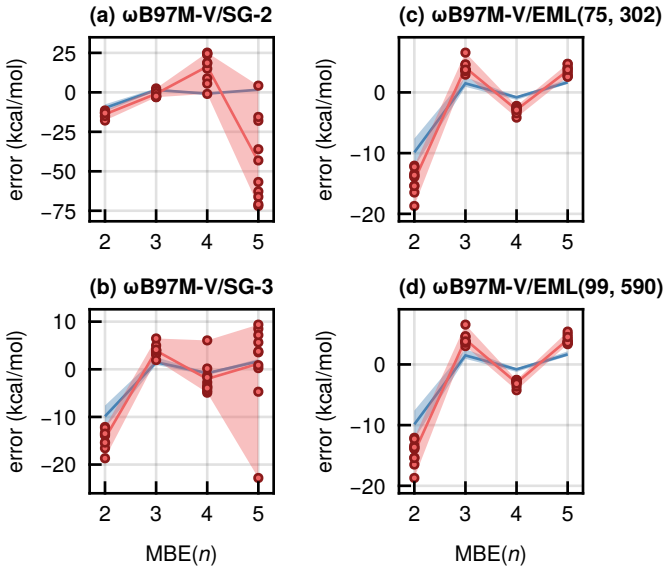

Figure S11: MBE(n) errors in ΔE_{int} (circles) for 10 $Cl^-(H_2O)_{15}$ cluster geometries, computed at the ωB97M-V/aug-cc-pVDZ level using various quadrature grids: (a) SG-2, (b) SG-3, (c) EML(75,302), and (d) EML(99,590). The red shaded region and solid line connect the range of the errors and their mean, for each value of n. The blue line and shaded region represent the HF/aug-cc-pVDZ error distribution from Fig. S1.

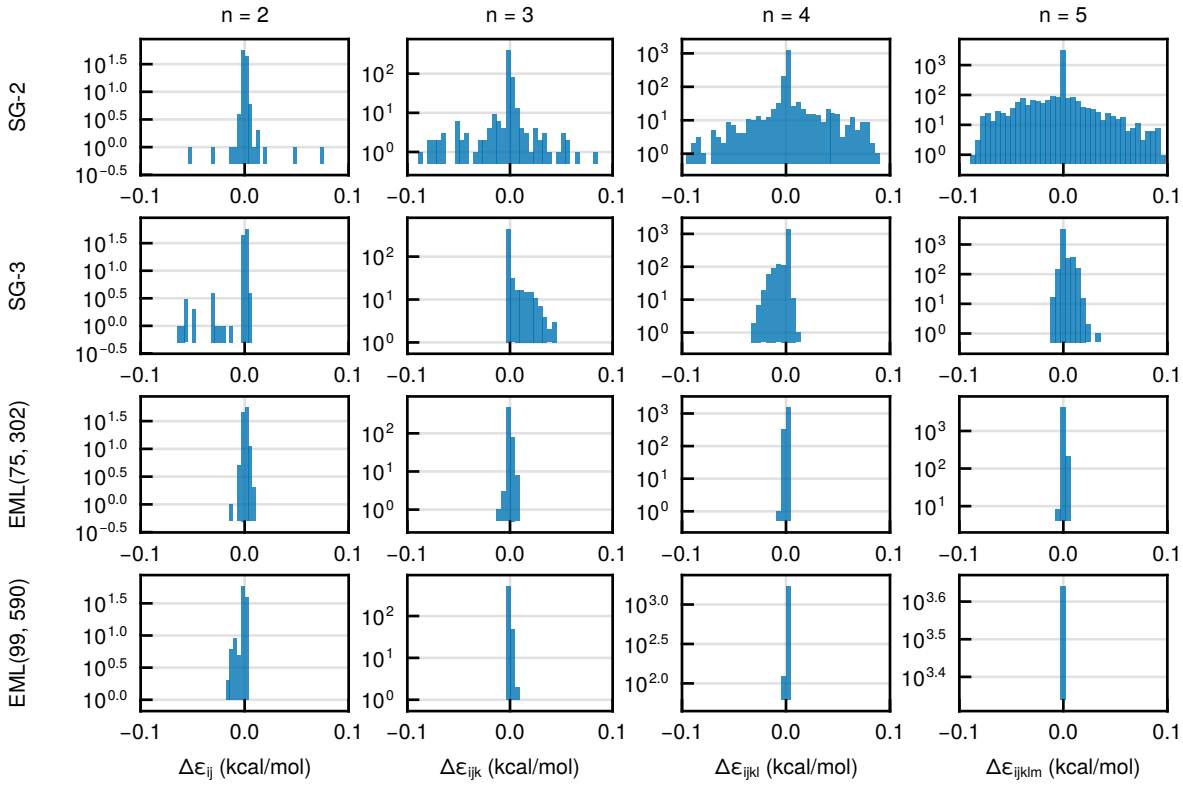

Figure S12: Histograms of grid-induced subsystem errors $\Delta\varepsilon_{IJ\ldots}$, for MBE($n$) corrections in $F^-(H_2O)_{15}$ clusters computed at the SCAN/aug-cc-pVDZ level with various quadrature grids.

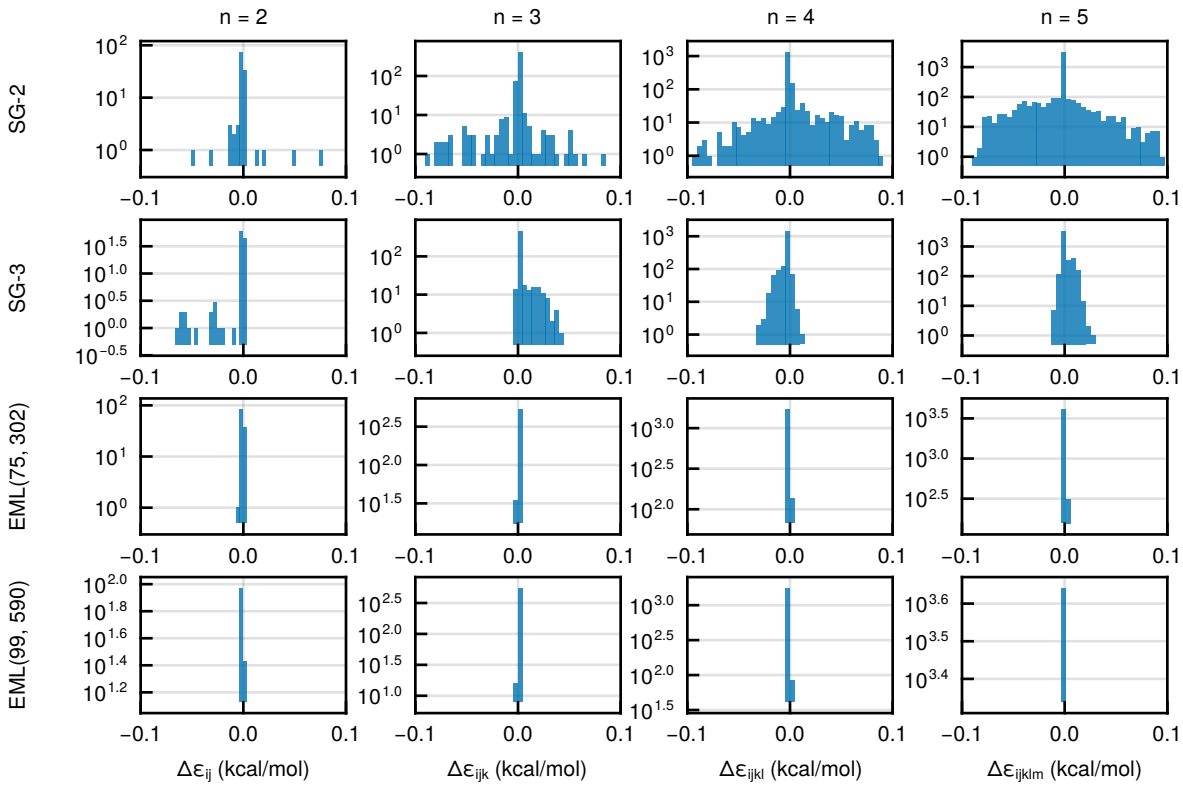

Figure S13: Histograms of grid-induced subsystem errors $\Delta\varepsilon_{IJ\ldots}$, for MBE($n$) corrections in $F^-(H_2O)_{15}$ clusters computed at the r^{2}SCAN/aug-cc-pVDZ level with various quadrature grids.